# Lawrence Berkeley National Laboratory
## Recent Work

**Title**
EFFECT OF VANADIUM ON DUAL PHASE Fe/Mn/Si/0.1C STEELS

**Permalink**
https://escholarship.org/uc/item/2wv7k5jk

**Author**
Nakagawa, A.H.

**Publication Date**
1981-06-01

# Lawrence Berkeley Laboratory

## UNIVERSITY OF CALIFORNIA

## Materials & Molecular Research Division

EFFECT OF VANADIUM ON DUAL PHASE Fe/Mn/Si/0.1C STEELS

Alvin H. Nakagawa
(M.S. thesis)

June 1981

## DISCLAIMER

# EFFECT OF VANADIUM ON DUAL PHASE Fe/Mn/Si/0.1C STEELS

Alvin H. Nakagawa

Materials and Molecular Research Division, Lawrence Berkeley Laboratory
and Department of Materials Science and Mineral Engineering
University of California, Berkeley, CA 94720

## ABSTRACT

This investigation is concerned with the effect of a 0.12% vanadium addition on a Fe/1.2Mn/0.6Si/0.1C dual phase steel. A comparison of structure and mechanical properties was made between these two alloys with and without vanadium. Two phase ($\alpha + \gamma$) and single phase ($\gamma$) annealing treatments were followed by a wide range of cooling rates.

In most cases, vanadium did not have a significant beneficial effect on the mechanical properties, although it changed the microstructure. The vanadium addition caused precipitation of vanadium carbide in the ferrite and a decrease in the ferrite grain size. During air cooling from the austenite phase field, it caused a small amount of martensite to form in an otherwise ferrite and pearlite microstructure. The precipitation strengthening effect of the vanadium carbides may have been too small to counteract the decrease in the amount of carbon strengthening of the martensite in the vanadium containing alloy. Oil quenching from the austenite phase field, gave the best mechanical properties for both the nonvandium and the vanadium bearing steels. In the latter case, the microstructure consisted of lath martensite plus bainitic ferrite-type structures.

# I. INTRODUCTION

The need for a strong formable steel for the automotive industry has been the driving force for numerous alloy development programs. One of the results has been the development of low carbon dual-phase (duplex ferrite-martensite) steels. Dual-phase structures can be produced by annealing in the $(\alpha + \gamma)$ region followed by cooling rates sufficient to transform the austenite to martensite[1,2]. Other industrial type processing of dual phase steels include hot rolling, continuous annealing, batch annealing[3], and continuous cooling from the austenite region[4]. As opposed to grain size control and carbide precipitation in HSLA steels, the major source of strengthening in the dual-phase steels is the incorporation of strong martensite in a ductile ferrite matrix[5].

The characteristics of dual phase steels are low yield strength to tensile strength ratios, continuous yielding behavior, high strain hardening rates and good ductility. The first two characteristics result from the large amount of fresh dislocations produced during the austenite to martensite transformation which occurs during cooling from the two phase region[4,6]. During tensile testing or forming deformation, continuity of strain between the hard martensite and soft ferrite requires that there be large amounts of inhomogeneous deformation in the ferrite. This causes a further increase in the dislocation density in the ferrite near the martensite and the results in a high rate of work hardening[4,6]. The transformations of any retained austenite also increases the number of dislocations[6] and the work hardening rate[7]. The high rate of work hardening suppresses necking, resulting in excellent uniform elongation values which in turn increases the total elongation[4,6].

Since the study of dual-phase steels was started here at Berkeley by

Thomas and Koo[2], the effects of different metallurgical variables such as martensite volume fraction[8], morphology[9], carbon content[8], and alloying additions[10,11,12] have been studied.

In this investigation, the effect of a strong carbide forming element viz. vanadium on a dual phase steel has been studied. The main objective is to determine its effect on tensile properties because of anticipated effects on the microstructure and hence to establish structure property relationships. In all of the above cases, the effect of vanadium was isolated in several different heat treatments by comparing the vanadium containing alloy with an identical alloy without vanadium. Besides the fundamental research reasons for this investigation, there are economic and resource conservation reasons for determining whether or not vanadium is a necessary alloying addition in this dual phase steel.

## II. EXPERIMENTAL PROCEDURE

### A. Materials Preparation

The alloys used in this investigation were vacuum induction melted at Lawrence Berkeley Laboratory in the form of 20 pound cylindrical ingots. The ingots were homogenized in argon at 1100°C for 24 hours. They were upset and cross-forged at 1100°C to 3" by 1" bars and then hot rolled at 1100°C to approximately 1/8". All of the above treatments were followed by air cooling. Oversized tensile blanks were cut from the flat plate with the tensile axis parallel to the rolling direction.

The chemical compositions of the two alloys as analyzed by wet chemical (C and Si) and X-ray spectroscopy (Mn and V) are given in Table 1.

### B. Heat Treatment

The hot rolled specimens were heat treated in a vertical tube furnace

under a flowing argon atmosphere. Four specimens were heat treated at the same time in a holder that kept them evenly spaced at right angles. Three specimens were used for tensile testing and the fourth was cut into pieces for optical, TEM and X-ray studies. The specimens were either intercritically annealed in the alpha + gamma phase field at 800°C or in the gamma region at 900°C. As shown in Fig. 1(a), the specimens were heated up to within 5°C of their final temperature after about 7 minutes. After a total holding time of 10 minutes, the specimens were dropped through the bottom of the furnace and subjected to either an agitated iced brine quench, an agitated oil quench, a forced air cool or a natural convection air cool.

The corresponding cooling rates from 800°C were measured by a thermocouple in the center of the specimen and recorded by a strip chart recorder. The results appear in Fig. 1(b). The average cooling rates from 800°C to 400°C for the iced brine quench, oil quench, forced air cool and air cool were found to be approximately 1000°C/sec, 100°C/sec, 5°C/sec and 3°C/sec respectively. The cooling rates from 900°C were found to be in the same range.

The calculated $M_s$ temperature for the alloys is 465°C[13]. When the alloys are held at 800°C, the microstructure is approximately 20% austenite. Assuming that the carbon is enriched to 0.5%, the calculated $M_s$ temperature becomes 350°C.

C. Mechanical Testing

Tensile properties were determined using 0.1" flat tensile bars with 1" gauge lengths. After heat treating, the oversize specimens were ground under flood cooling to ASTM specification E8-69 shown in Fig. 2. The

specimen thickness is 0.100". Approximately 35 mils of material was ground from the surface of the specimens to remove any decarburized material. The decarburization was less than 25 mils.

Testing was done at room temperature on an Instron testing machine with a cross-head speed of 0.05/min and a full scale load of 1000kg. The total elongations were determined by measuring 1" marks on the gauge before and after testing. The reduction in area was based on measurements of the gauge dimensions before and after testing with a micrometer and then an optical microscope equipped with a vernier translating stage. The rest of the properties were determined from the curves produced by the testing machine's chart recorder. The yield strengths were determined by the 0.2% offset method.

D. Metallography

1. Optical Metallography. Specimens for optical metallography were cut from the extra tensile blanks under flood cooling. After mounting in either bakelite or kold-mount, they were rough ground on a flood cooled 240 grit belt and then hand ground on wet silicon carbide paper from 240 to 600 grit. The final polish was done with 1μm diamond paste on a polishing wheel and then with 0.3μm alumina on a felt cloth. After the microstructural details were revealed by etching in a 2% nital solution, the specimens were observed in a Zeiss Ultraphot II metallograph. Volume fractions were determined by a point fraction method[14].

2. Transmission Electron Microscopy. Thin foils for transmission electron microscopy were obtained from part of the extra tensile blank. Slices of approximately 25 mils were slow cut with a 1/32" silicon carbide abrasive disc under flood cooling. The slices were then given a uniform

thickness by removing 0.5 mils per pass with a flood cooled surface grinder. The slices were chemically thinned to 2-3 mils at room temperature in a solution of 96 ml of 30% $H_2O_2$ and 4 ml of 48% HF. After the 3 mm discs were spark cut from these slices, they were hand ground on 600 grit to remove any oxide layer. The discs were polished to thin foils at room temperature in a twin jet electropolisher using a chromic acetic acid solution of 75 gm $CrO_3$, 400 ml $Ch_3COOH$ and 21 ml distilled water. Polishing potentials from 35-50 volts were used. The thin foils were stored in 200 proof ethyl alcohol and later examined in a Hitachi HU125 or a Philips EM301 electron microscope at an accelerating voltage of 100 kV. STEM analysis was done with a Philips EM400 electron microscope.

3. Scanning Electron Microscopy. Fractography was conducted on the broken surfaces of the tensile specimens using an AMR-1000 scanning electron microscope operating at 20 kV. The gauge sections of the specimens were removed with a hand saw and clamped in a specimen holder for observations.

E. X-ray Analysis

X-ray diffraction was used to determine the volume fraction of retained austenite in the steels. Part of the extra tensile blanks were used for this purpose. A surface grinder with flood cooling was used to remove 25 mils from each side. The specimens were then wet ground on silicon carbide paper from 240 to 600 grit. One side was chemically thinned at room temperature in a solution of 96 ml of 30% $H_2O_2$ and 4 ml of 40% HF while the other side was protected by a lacquer.

The resulting shiny surface was examined with a General Electric Diano X-ray diffractometer using filtered Mo $K_\alpha$ radiation. The specimens

were scanned at 0.2°/min from $2\theta = 20°$ to $2\theta = 40°$ to include the

$\gamma_{200}$, $\alpha_{200}$, $\gamma_{220}$, $\alpha_{211}$ and $\gamma_{311}$ peaks following the procedure outlined

by Miller[15]. The specimens were examined with their rolling directions

both parallel and perpendicular to the X-ray beams.

## III. Results and Discussion

### A. Microstructure

1. Effect of Heat Treatment. A summary of the optical and TEM

observations of the microstructures appears in Table II. The starting

microstructures (as hot rolled) for the two steels are shown in Fig. 3.

They consist mainly of proeutectoid ferrite plus a second phase or pear-

lite. The grain size is approximately the same in the two steels. The

only difference between the two is the banding in the base steel (MB).

When the steels are heated to 800°C, the austenite nucleates

heterogeneously at $Fe_3C$ particles located on ferrite/ferrite grain boun-

daries[15], then grows to approximately 20% of the total volume as determined

by the tie line in the $(\alpha + \gamma)$ region of the iron-carbon-manganese

equilibrium phase diagram. The actual amount is slightly less than

equilibrium because of the short annealing time. It is not necessary to

know the boundaries of the $(\alpha + \gamma)$ phase field since the annealing

temperature for a specific volume fraction can be determined by a few

test samples.

Quenching in agitated iced brine (800°C IBQ) transforms the austenite

which forms during the annealing into martensite as can be seen in Fig. 4.

The fine globules of martensite decorate the ferrite grain boundaries.

The austenite grows along the boundaries rather than into the ferrite

grains since carbon diffusion is much more rapid parallel to rather than

perpendicular to grain boundaries[16]. Figs. 5 and 6 show the high concentration of dislocations at the ferrite/martensite interface that are typical in dual-phase steels. In Figure 5 one can see the two regions of ferrite in alloy MV. Near the martensite there is a precipitate free area with a high density of dislocations. Further into the ferrite, there are less dislocations in the precipitate hardened area.

The martensite consists of lath and some twinned martensite. The presence of twinned martensite is to be expected since the carbon content is greater than 0.4%[17].

Oil quenching from 800°C (800°C OIL) produces the microstructure shown in Fig. 7. The volume fraction and distribution of martensite is nearly the same as above.

Upon forced air (800°C FAC) and natural convection air cooling (800°C AC) from 800°C, the austenite which forms during two phase annealing transforms to additional proeutectoid ferrite and then to pearlite and maybe some upper bainite but no martensite or lower bainite. The resulting microstructures are shown in Fig. 8. When the steels are heated to 900°C, the austenite nucleates and grows to nearly 100% of the total volume since 900°C is in the austenite phase field for the compositions used.

Quenching in oil (900°C OIL) causes some proeutectoid ferrite to form. The remaining austenite then tranforms to martensite to give the micro-structures shown in Fig. 9. Although most of the second phase consists of lath martensite, there is also a small amount of bainite as shown in Fig. 10. Upon forced air (900°C FAC) and natural convection air cooling (900°C AC) from 900°C, pearlite formation again follows the formation of pro-eutectoid ferrite. The microstructures for 900°C AC are shown in Fig. 11.

Figs. 12 and 13 show the pearlite and surrounding ferrite. Considerable precipitation is visible in the proeutectoid ferrite of Fig. 12, but the ferrite in Fig. 13 appears to be much "cleaner". Fig. 14 is a TEM micrograph of the MB 900 AC steels showing the fine precipitates found in varying amounts in all of the specimens. The microstructures of the 900°C AC specimens are similar to those of the 800°C AC treatment except that all of the ferrite forms during cooling since no ferrite can be retained during annealing in the austenite range. In the forced air and air cool treatments from both 800°C and 900°C, the volume fraction of the pearlite is approximately 10%.

2. Effect of Vanadium. In steels, vanadium tends to form carbides, the equilibrium form being $V_4C_3$. Besides increasing the strength of the ferrite by precipitation hardening, other effects of vanadium are to increase the hardenability and to reduce the austenite grain size[18]. Hardenability is increased by the competition of the formation of vanadium carbide with that of cementite, thus retarding higher transformation temperature products. Vanadium carbides cause smaller austenite grain sizes during controlled rolling by providing more nucleation sites for recrystallization and by retarding grain growth.

Although vanadium is known to be an effective grain refining alloying addition, it does not seem to have much of an effect on the grain size of the as-received (hot rolled) material as shown in Fig. 3. However, the optical micrographs of the heat treated steels, Figs. 4, 7-9 and 11, show the effectiveness of vanadium in causing a smaller grain size.

For example, in the 800°C iced brine quench specimen, Fig. 4, t/ austenite (martensite) and ferrite grains are noticeably smaller in

vanadium containing alloy (b). Since the austenite grains are surrounded
by ferrite during two-phase annealing, grain growth in the usual sense
(e.g. austenite grain boundary motion) cannot occur. Instead, a coarsening
reaction would have to take place. In this case, the effect of the vana-
dium is to reduce the diffusivity of carbon because of its carbon affinity
and size difference with respect to iron. The result is a decrease in
the rate of the coarsening reaction.

In the case of the ferrite, there are many ferrite/ferrite grain
boundaries. In the alloy without vanadium, there are fewer austenite
particles as a result of the coarsening reaction and there are no VC
precipitates. This allows the ferrite/ferrite grain boundaries to move
freely causing the ferrite grains to be larger in the alloy without
vanadium as shown in Fig. 4.

During 900°C annealing, the microstructure consists of only
austenite, thus reduction of austenite grain growth during annealing
and increased ferrite nucleation during cooling are probably the mech-
anisms by which vanadium caused the smaller grain sizes in alloy MV as
compared to MB after 900°C annealing. The nucleation of austenite during
heating and renucleation of ferrite during cooling together with the
effect of vanadium account for the smaller grain size of the vanadium
containing alloy after heat treatment as compared to the as received
material.

In the transmission electron microscope, one can see that vanadium
causes significant differences in the precipitate morphology. Fig. 15 shows
the interphase precipitation found only in the vanadium containing alloy.
It is well known that carbide forming elements such as vanadium promote

this type of precipitation[19]. Another difference is shown in Fig. 16. In addition to the pearlite found in the 900°C AC specimens, some twinned plate martensite was found in the vanadium containing alloy. This may be due either to the hardenability effect of vanadium or to some segregation of manganese or carbon caused by the vanadium. Although the fine precipitates shown in Figs. 12 and 14 were found in all of the treatments, the density of the precipitates was much higher in the vanadium containing alloys. No difference was found between the two alloys in the 900°C OIL heat treatment.

Table II summarizes the effect of vanadium on the microstructure of the steel.

STEM analysis of the vanadium containing alloy with the 800°C iced brine quench heat treatment did not detect any vanadium partitioning between the ferrite and martensite. This was probably because the amount of vanadium in the alloy (0.13 at %) was below the detectability level for the instrument.

3. _Fractography_. A SEM micrograph of the dimpled structure of the tensile specimen fracture surface appears in Fig. 17. This is for the 800°C IBQ treatment, but the ductile fracture appearance is typical of all the specimens tested.

4. _Retained Austenite_. There have been several reports of retained austenite in dual-phase steels[3,6,16,20-24]. The reported amounts of retained austenite vary from less than 1%[16] to as much as 12.6%[23] with most reporting approximately 5% for compositions similar to the one being studied. The volume percent was found to increase with the annealing temperature[3,24] and the concentration of vanadium[23]. The cooling rate

may have an effect, but it has not been well established. One report found that the amount of austenite increased with decreasing cooling rates[23] while another reported a maximum in the volume percent at a cooling rate of 50°C/sec.[6]. There have been reports of thermally stable[20,21] as well as thermally unstable[22,23] retained austenite. In most cases, it was not found to be mechanically stable. The effect on mechanical properties is also unclear. One report concluded that the amount is too small to have any effect[24] and another found that it transforms too easily to have any effect[22]. On one hand, it was concluded that the ductility increases with the volume percent of retained austenite[23] and on another that the strain hardening rate increased with the amount of retained austenite[21].

X-ray analysis of the vanadium containing alloy after all five heat treatments failed to detect any retained austenite. No X-ray analysis was done on the alloy without vanadium. TEM studies also failed to reveal any retained austenite in either alloy. Thus in the present investigation it can be concluded that if there is retained austenite the amount must be less than $\sim$1%.

In this investigation, the retained austenite volume fraction may have been too low to detect by X-ray diffraction because of the heat treatment used. It is possible that the discrete particle retained austenite which was reported in the literature results from a high degree of partitioning of carbon and manganese, both of which are austenite stabilizers[25-27]. Furukawa et al.[21] purposely obtained an enriched second phase prior to heat treatment by careful control of the coiling temperature following the hot rolling treatment. The short annealing time (2 minutes) and low annealing temperature (750°C) used in that

investigation helped maintain the segregation in the austenite. Upon cooling, some of this enriched austenite is retained. This investigation used a simple hot rolling and a 10 minute anneal at 800°C or 900°C. Some investigators[6,28] reporting retained austenite in their dual-phase steel used a neutral salt pot for their heat treatments which gives a much more rapid heating rate than the tube furnace used in the present investigation. This would result in a higher nucleation rate for the austenite, thus resulting in a large number of small austenite particles. It has been speculated that these particles are stabilized and therefore retained because of their small size through restraint or lack of nucleation site.

B. Mechanical Properties

1. <u>Effect of Heat Treatment</u>. A summary of the tensile test data appears in Table III. For each heat treatment, the data is given for the base alloy (MB) and the vanadium containing alloy (MV). There is a third row designated by $\Delta_V$ which indicates the changes in mechanical properties due to the addition of vanadium.[29]

For steels given the 800°C annealing treatment, one can see the effect of different cooling rates on dual-phase steels. As the cooling rate decreases from iced brine quench, to oil quench, to air cool, there is as expected, a decrease in the ultimate tensile strength (from $\sim$ 110ksi down to $\sim$ 80 ksi) and an increase in total elongation (from $\sim$20% up to $\sim$30%). The uniform yielding characteristics give way to the undesirable Lüders strain as the second phase changes from martensite to pearlite. Somewhere between cooling rates of 100°C/sec and 5°C/sec, the volume fraction of martensite goes below the minimum requirement of 10% for

continuous yielding behavior[3]. There is a decrease in the yield strength
following iced brine quench compared to oil quenching, because the slower
cooling rate reduces the hardening effect of the interstitial carbon[21],
but the yield strength rises for the air cooling treatments because there
no longer is any martensitic transformation to produce the fresh, mobile
dislocations expected from the transformation strain.

The change to the higher annealing temperature from 800°C to 900°C
results in a higher strength upon oil quenching (from ∿ 90ksi up to ∿ 115ksi)
and lower values of elongation (from ∿ 28% down to ∿ 23%). The results of
this 900°C OIL treatment are rather interesting because although oil
quenching from the austenite region is unlike any conventional dual-phase
treatment, it yields better values of both strength and ductility than
the 800°C IBQ treatment. Of all the treatments used, this one gave the
highest value of UTS x Total elongation.

In comparing the 900°C OIL to the 800°C OIL results, the increase in
strength comes from the increase in the volume fraction of martensite.
The higher values of ductility than expected for such a large volume
fraction of martensite result from the change in the martensite morphology
as the austenite carbon content changed from 0.5% to 0.1%. The 800°C
IBQ specimen contained a mixture of lath and twinned martensite, while the
900°C OIL specimen contained a mixture of lath martensite and upper
bainite. The small amount of proeutectoid ferrite also added to the
ductility.

2. <u>Effect of Vanadium</u>. A comparison of the stress strain curves
for steels with and without vanadium appears in Fig. 18. Overall, the
effect of vanadium is not significant in the heat treatments used. The

two minor exceptions are the 800°C IBQ and 800°C OIL treatments. In 800°C IBQ, (Fig. 18(a)), the yield and tensile strength is lowered by 7 ksi and 9 ksi respectively, while the elongations remain the same. In 800°C OIL, (Fig. 18(b)), the effect is the opposite. The yield and tensile strengths increase 7 ksi and 10 ksi respectively while the elongations decrease by approximately 5%.

One possible cause for the lower tensile strength of the vanadium containing alloy in the 800°C IBQ treatment is the lower amount of carbon available for the major strengthener, the martensite. A small factor contributing to this lower amount is the overall carbon content of the alloys. As shown in Table 1, the alloy without vanadium has 0.12% carbon, while the vanadium containing alloy has only 0.1% carbon. However, this effect is small since the 0.02 weight percent difference results in only a 4% change in the volume fraction of martensite at the same 800°C annealing temperature. Using the law of mixtures[8] as a guide, a rough calculation approximates the change in strength as 5 ksi. The effect is probably much less.

The effect of the vanadium is much greater. The first effect is on the phase diagram. Vanadium expands the $(\alpha + \gamma)$ phase field since it is a ferrite former and it depresses the $a_{c_1}$ by 50°C per 1% V[30]. These changes affect the volume percent as well as the composition of the martensite. The second effect is the decrease in solid solution carbon content due to the carbon formation of vanadium carbides. This is probably the major cause of the lower strenth in the 800°C IBQ treatment.

Normally, one would expect the strength to increase because of the vanadium carbides. The increase may have been too small to overcome the

loss in strength caused by the decrease in carbon because of coarse carbides left from hot rolling.

In the 800°C OIL treatment, the slower cooling rate may have allowed more time for the formation of carbides and strengthened proeutectoid ferrite. This increased the strength of the vanadium containing alloy efficiently enough to overcome the lower carbon level.

In the 800°C AC data, one can see that the yield strength of the vanadium containing alloy is higher than that of the base alloy. This is probably due to the increased precipitation in the ferrite. The lower yield strength of the vanadium containing alloy in the 900°C AC data may be due in part to some mobile dislocations in the ferrite originating from the strain associated with the transformation of austenite to a small amount of martensite in the vanadium containing alloy.

The key point is that a vanadium addition is not necessary to achieve superior tensile properties for the 900°C OIL treatment. The alloy without vanadium has properties that are essentially identical to those of the vanadium-containing alloy.

## IV. Conclusions

Based on the present investigation of the effect of a 0.12%V addition on a dual-phase Fe/Mn/Si/0.1C alloy, the following conclusions can be drawn:

1. The addition of 0.12%V caused a decrease in the ferrite grain size, caused interphase precipitation of carbides, caused an increase in the density of fine precipitates in the ferrite and, in air cooled specimens, caused the formation of a small amount of martensite in the otherwise pearlitic structure.

2. However, despite the changes in microstructure, the vanadium addition did not cause any significant beneficial effect on the tensile properties.

3. The precipitation strengthening if the vanadium containing alloy may have been counteracted by the lower volume fraction of martensite and the lower amount of soluble carbon available in martensite because of the carbon tied up in the precipitates.

4. The 900°C oil quench treatment produced the best properties even though quenching in oil from the austenite phase field is not a conventional dual-phase heat treatment.

5. In this superior heat treatment, the properties and micro-structures of the two alloys were almost identical.

6. Air cooling and forced air cooling from the two phase $(\alpha + \gamma)$ region and the single phase austenite region produced a predominantly ferrite plus pearlite microstructure with undesirable discontinuous yielding.

Don Krieger and Weyland Wong is recognized.

Thanks are also due to Madeline Moore and Kathleen Brusse for typing this manuscript.

## REFERENCES

1. M. S. Rashid, "GM980X - A Unique High Strength Steel with Superior Formability", SAE 760206, 1976.

2. J. Y. Koo and G. Thomas, "Thermal Cycling Treatments and Micro-structures for Improved Properties of Fe-0.12%C-0.5%Mn Steels," Mat. Sci. and Eng. 24, 187 (1976).

3. J. M. Rigsbee, J. K. Abraham, A. T. Davenport, J. E. Franklin and J. W. Pickens, "Structure-Processing and Structure-Property Relationships in Commercially Processed Dual-Phase Steels", p. 304 in Structure and Properties of Dual-Phase Steels, R. A. Kot and J. W. Morris, eds., AIME, New York, N. Y. , 1979.

4. J. H. Bucher and E. G. Hamburg, "High Strength Formable Sheet Steel", SAE 770164, 1976.

5. J. Y. Koo and G. Thomas, "Design of Duplex Low Carbon Steels for Improved Strength: Weight Applications", p. 40 in Formable HSLA and Dual-Phase Steels, A. T. Davenport, ed., AIME, New York, N. Y., 1979.

6. D. K. Matlock, G. Krauss, L. F. Ramos and G. S. Huppi, "A Correlation of Processing Variables with Deformation Behavior of Dual Phase Steels", p. 62 in Structure and Properties of Dual-Phase Steel, R. A. Kot and J. W. Morris, eds., AIME, New York, N. Y., 1979.

7. D. Webster, "Development of a High Strength Stainless Steel with Improved Toughness and Ductility", Met. Trans. 2, 2097 (1971).

8. J. Y. Koo, M. J. Young, and G. Thomas, "On the Law of Mixtures in Dual-Phase Steels", Met. Trans. A 11A, 852 (1980).

9. N. J. Kim and G. Thomas, "Effects of Morphology on the Mechanical Behavior of a Dual-Phase Fe/2Si/0.1C Steel", Met. Trans. A 12A, 483 (1981).

10. P. K. Costello, "Design of Duplex Low Carbon Steels with Carbide Forming Elements", M. S. Thesis, University of California, Berkeley, LBL-8628, December 1978.

11. T. J. O'Neill, J. Y. Koo and G. Thomas, "Microstructure and Properties of Dual Phase Steels containing Silicon, Aluminum and Molybdenum, submitted to Met. Trans., November 1980.

12. J. S. Gau, "Mechanical Properties and Microstructure of a Low Carbon Steel with Nb.", M. S. Thesis, University of California, Berkeley, LBL-12058, April 1981.

13. R. E. Reed-Hill, Physical Metallurgy Principles, 2nd ed., D. Van Nostrand and Co., New York, 1973.

14. E. E. Underwood, "Applications of Quantitative Metallography", in ASM Metals Handbook, Vol. 8, p. 37 (1961).

15. R. L. Miller, "A Rapid X-ray method for the Determination of Retained Austenite", Trans. ASM 57, 839 (1964).

16. C. I. Garcia and A. J. DeArdo, "The Formation of Austenite in Low Alloy Steels", p. 40 in Structure and Properties of Dual-Phase Steels, R. A. Kot and J. W. Morris, eds., AIME, New York, N. Y., 1979.

17. B. V. N. Rao, "Role of Quaternary Additions on Dislocated Martensite Retain Austenite and Mechanical Properties of Fe/Cr/C Structural Steels," Ph.D. Thesis, University of California, Berkeley, LBL-7361, (1978).

18. J. F. Butler and J. H. Bucher, "Vanadium HSLA Steels with Superior Formability", in Production and Properties of Vanadium Dual Phase Steels and Cold Pressing Steels in the Automobile Industry, Proceedings of a seminar in Berlin, Vanadium International Technical Committee, October 1978.

19. R. W. K. Honeycombe, "Transformation from Austenite in Alloy Steels", Met. Trans. 7A, p. 915 (1976).

20. A. R. Marder, "Factors Affecting the Ductility of 'Dual-Phase' Alloys", in Formable HSLA and Dual-Phase Steels, A. T. Davenport ed., AIME, New York, N. Y., 1979, p. 89.

21. T. Furukawa, H. Morikawa, H. Takeuchi and K. Koyama, "Process Factors for Highly Ductile Dual-Phase Sheet Steels", p. 281 in Structure and Properties of Dual-Phase Steels, R. A. Kot and J. W. Morris, eds., AIME, New York, N. Y. 1979.

22. G. T. Eldis, "The Influence of Microstructure and Testing Procedure on the Measured Mechanical Properties of Heat Treated Dual-Phase Steels," p. 202 in Structure and Properties of Dual-Phase Steels, R. A. Kot and J. W. Morris, eds., AIME, New York, N. Y. 1979.

23. K. Nakaoka, Y. Hosoya, M. Ohmura and A. Hishimoto, "Reassessment of the Water-Quench Process as a Means of Producing Dual-Phase Formable Sheet Steels", p. 330 in Structure and Properties of Dual-Phase Steels, R. A. Kot and J. W. Morris, eds., AIME, New York, N. Y., 1979.

24. G. R. Speich and R. L. Miller, "Mechanical Properties of Ferrite-Martensite Steels," p. 145 in Structure and Properties of Dual-Phase

Steels", R. A. Kot and J. W. Morris, eds., AIME, New York, N. Y.,
1979.

25. P. G. Shewmon, Transformations in Metals, McGraw-Hill Book Co.,
New York, 1969.

26. B. Edmondson and T. Ko, "Spontaneous Deformation of Austenite
During Martensitic Transformations", Acta Met., 2, 235 (1954).

27. K. W. Andrews, "The Calculation of Transformation Temperatures
and Austenite-Ferrite Equilibria in Steels", JISI 184, 414 (1956).

28. W. R. Cribb and J. M. Rigsbee,"Work-Hardening Behavior and its
Relationship to the Microstructure and Mechanical Properties of
Dual-Phase Steels", in Structure and Properties of Dual-Phase
Steels, R. A. Kot and J. W. Morris, eds., AIME, New York, N. Y.,
1979.

29. W. C. Leslie and R. L. Miller, "The Stabilization of Austenite
by Closely-Spaced Boundaries", Trans. ASM 57, 972 (1964).

30. E. C. Rollason, "Fundamental Aspects of Molybdenum on Transforma-
tion of Steel", Climax Molybdenum Co., No. M89 12/72 IOM.

FIGURE CAPTIONS

Fig. 1.  Heating curve (a) and cooling curve (b) of specimens during
heat treatment as measured by a thermocouple inside an extra
tensile test blank.

Fig. 2.  Drawing of ASTM specification E8-69 flat tensile specimen.
The specimen thickness is 0.100".

Fig. 3.  Optical microscopes of as received microstructure: (a) Base
(MB), (b) Base + V (MV). Nital etch.

Fig. 4.  Optical micrographs of 800°C iced brine quench specimens:
(a) Base, (b) Base + V. Nital etch.

Fig. 5.  TEM micrograph of MV 800°C IBQ showing dislocations in ferrite
near martensite and interaction with precipitates.

Fig. 6.  TEM micrograph of MB 800°C IBQ showing dislocations in ferrite
near martensite.

Fig. 7.  Optical micrographs of 800°C oil quench specimens: (a) Base,
(b) Base + V. Nital etch.

Fig. 8.  Optical micrographs of 800°C air cool specimens: (a) Base,
(b) Base + V. Nital etch.

Fig. 9.  Optical micrographs of 900°C oil quench specimens: (a) Base,
(b) Base + V. Nital etch.

Fig. 10. TEM micrograph of bainite in the MV 900°C oil quench specimen:
(a) bright field and (b) SAD showing cementite [$\bar{1}$00] with
ferrite [$\bar{1}$01].

Fig. 11. Optical micrographs of 900°C air cool specimens: (a) Base,
(b) Base + V. Nital etch.

Fig. 12. TEM micrograph of pearlite in MV 900° AC with precipitation.

## Table I

### Alloy Compositions (wt. pct.)

| Alloy Designation | C | Si | Mn | V | Fe |
|---|---|---|---|---|---|
| MB | 0.12 | 0.57 | 1.16 | <0.005 | Bal |
| MV | 0.10 | 0.57 | 1.16 | 0.12 | Bal |

TABLE II Summary of Microstructures

| Heat Treatment | Alloy | "Second Phase" | Interface Precipitation | Fine Precipitation (in ferrite($\#/cm^3$) | Type of ferrite |
|---|---|---|---|---|---|
| 800IBQ | MB | Martensite | No | high $3.5 \times 10^{15}$ | retained +new |
| | MV | Martensite | Yes | very high $4.5 \times 10^{15}$ | retained |
| 9000IL | MB | Martensite some upper bainite | No | low $\sim 0$ | new |
| | MV | Martensite some upper bainite | No | low $\sim 0$ | new |
| 800AC | MB | Pearlite (upper bainite) | No | very low 200 $2.5 \times 10^{14}$ | retained +new |
| | MV | Pearlite (upper bainite) | Yes | low $5 \times 10^{14}$ | retained +new |
| 900AC | MB | Pearlite (upper bainite) | No | very low $2.5 \times 10^{14}$ | new |
| | MV | 80% Pearlite+Bainite 20% Martensite | Yes | medium $2.0 \times 10^{15}$ | new |

Table III

Tensile Properties

| Heat Treatment | Alloy | Y.S. ksi (MPa) | U.T.S. ksi (MPa) | Y.S./U.T.S. | Uniform Elongation (%) | Total Elongation (%) | Luders Strain (%) | Reduction in Area (%) | U.T.S. x Total Elong. ksi x % (GPa x %) |
|---|---|---|---|---|---|---|---|---|---|
| 800°C IBQ | MB | 65(448) | 114(785) | 0.57 | 13 | 19 | 0 | 50 | 2170(14.9) |
| | MV | 58(400) | 105(723) | 0.55 | 13 | 19 | 0 | 54 | 2000(13.7) |
| | Δv | -7(-48) | -9(-62) | +0.02 | 0 | 0 | 0 | +4 | -170(-1.2) |
| 800°C OIL | MB | 47(324) | 86(589) | 0.55 | 23 | 30 | 0 | 41 | 2580(17.7) |
| | MV | 54(369) | 96(661) | 0.56 | 17 | 25 | 0 | 47 | 2400(16.5) |
| | Δv | +7(+45) | +10(+72) | +0.01 | -6 | -5 | 0 | +6 | -180(-1.2) |
| 900°C OIL | MB | 77(531) | 118(813) | 0.65 | 12 | 22 | 0 | 75 | 2596(17.9) |
| | MV | 79(544) | 115(795) | 0.68 | 12 | 23 | 0 | 71 | 2650(18.3) |
| | Δv | +2(+13) | -3(-18) | +0.03 | 0 | +1 | 0 | -4 | +54(+0.4) |
| 800°C FAC | MB | 48(331) | 76(521) | 0.64 | 18 | 28 | 0.7 | 81 | 2130(14.6) |
| | MV | 51(354) | 76(526) | 0.67 | 18 | 31 | 1.4 | 83 | 2360(16.3) |
| | Δv | +3(+23) | 0(+5) | +0.03 | 0 | +3 | +0.7 | +2 | +230(+1.7) |
| 900°C FAC | MB | 56(386) | 77(533) | 0.72 | 19 | 33 | 2.5 | 84 | 2540(17.6) |
| | MV | 56(386) | 77(503) | 0.77 | 21 | 36 | 3.2 | 84 | 2630(18.1) |
| | Δv | 0(0) | -4(-30) | +0.05 | +2 | +3 | +0.7 | 0 | +90(+0.5) |
| 800°C AC | MB | 50(345) | 77(531) | 0.65 | 17 | 29 | 1.1 | 80 | 2230(15.4) |
| | MV | 58(396) | 75(517) | 0.77 | 17 | 29 | 2.4 | 83 | 2180(15.0) |
| | Δv | +8(+51) | -2(-14) | +0.12 | 0 | 0 | +1.3 | +3 | -50(-0.4) |
| 900°C AC | MB | 54(370) | 75(517) | 0.72 | 21 | 35 | 2.7 | 84 | 2630(18.1) |
| | MV | 50(341) | 76(520) | 0.66 | 21 | 34 | 1.2 | 80 | 2580(17.7) |
| | Δv | -4(-29) | +1(+3) | -0.06 | 0 | -1 | -1.5 | -4 | -50(-0.4) |

## HEATING CURVE

FURNACE TEMPERATURE
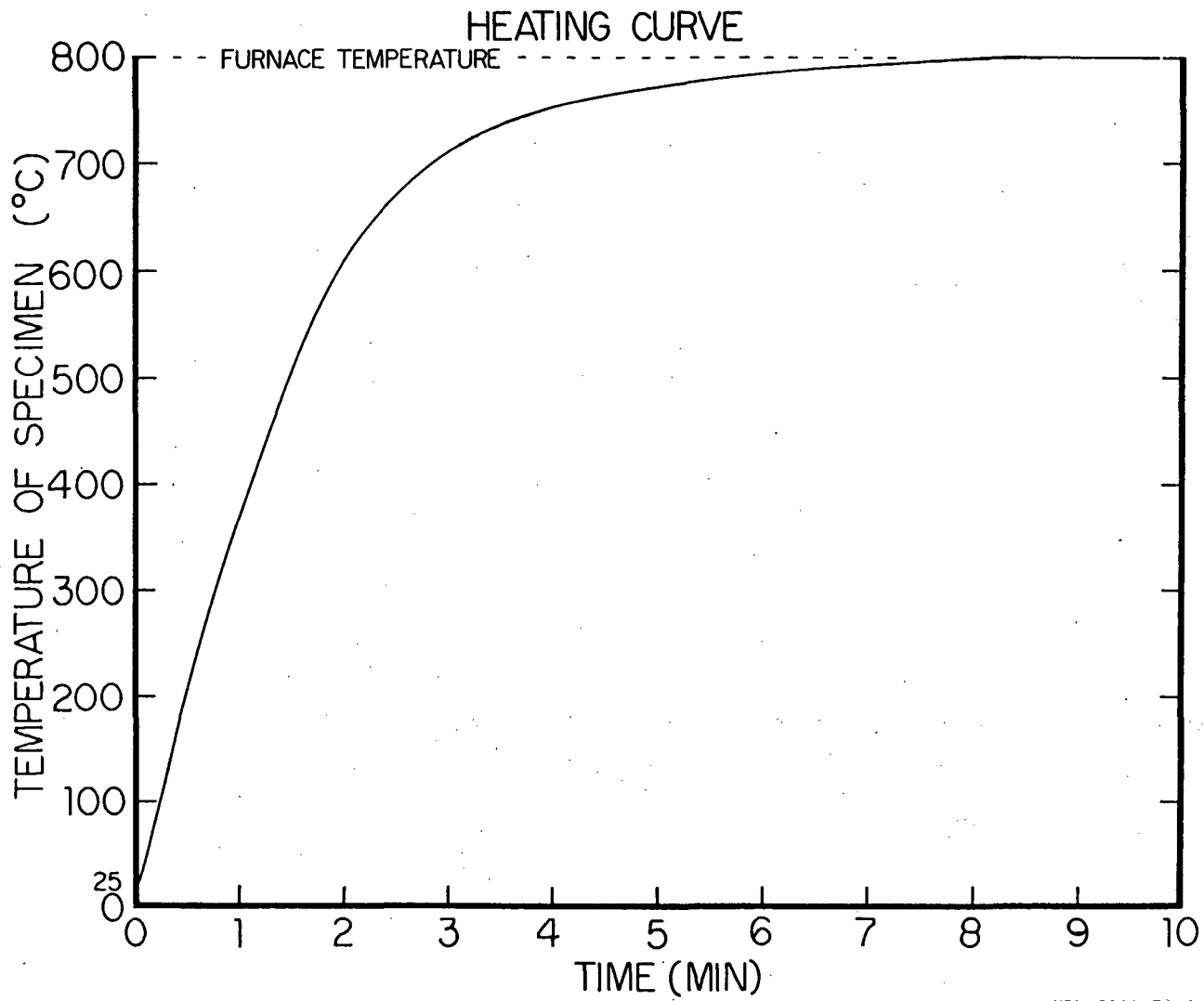
Fig. 1a
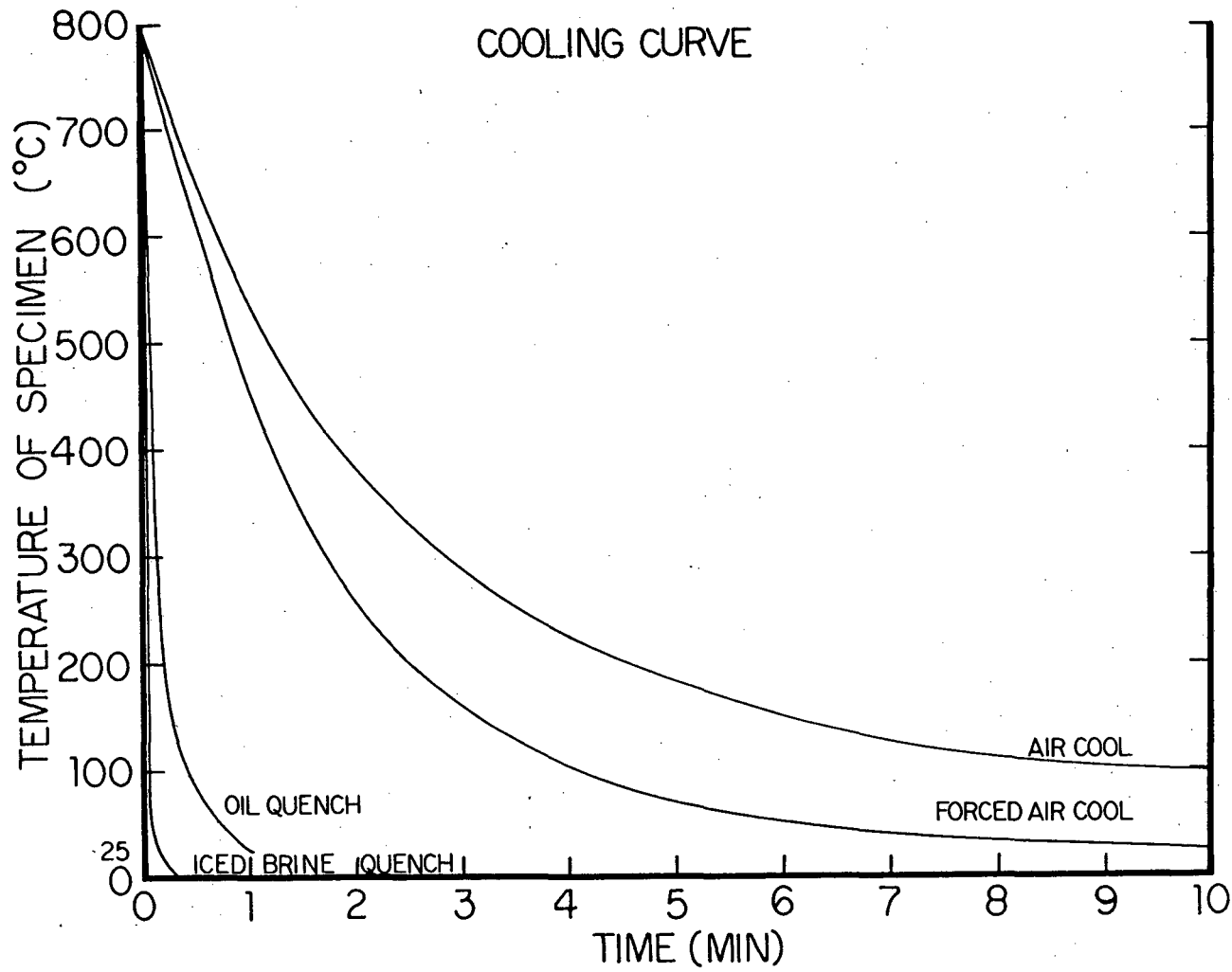
Fig. 1b

XBL 8011-7413
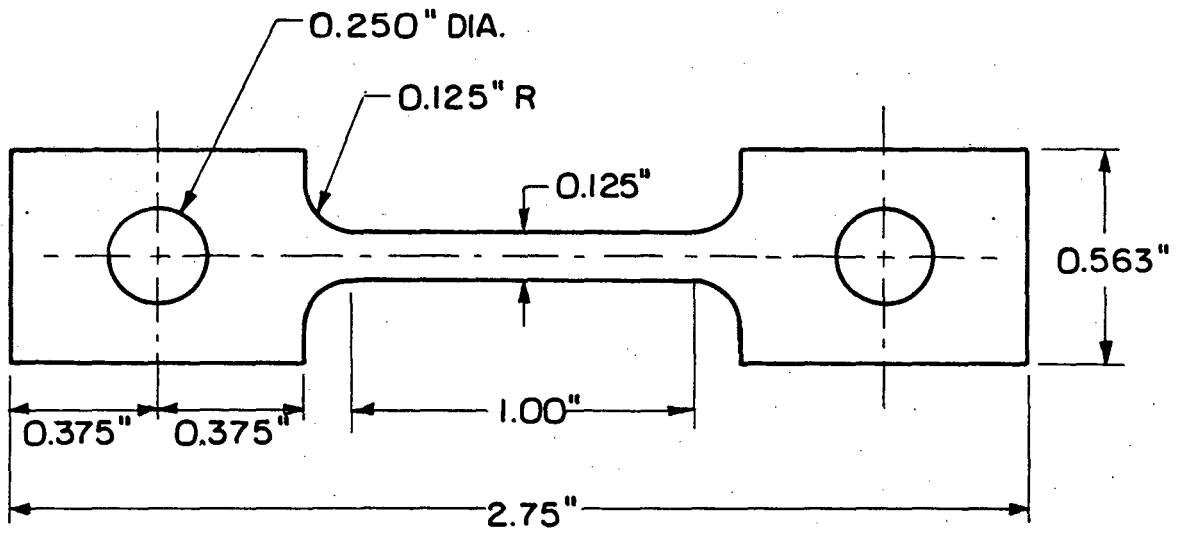
XBL737-6444

Fig. 2
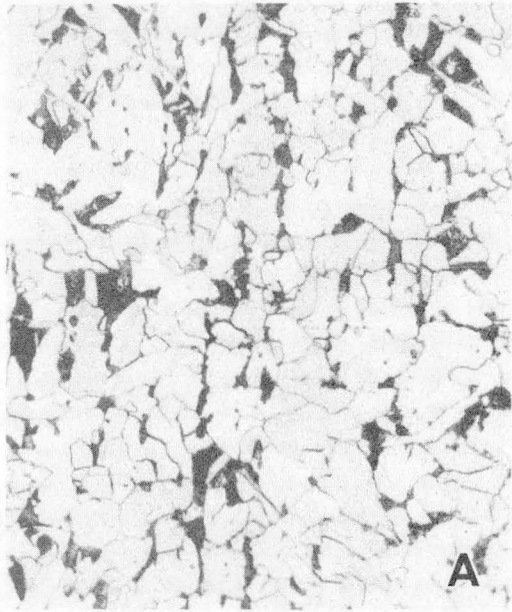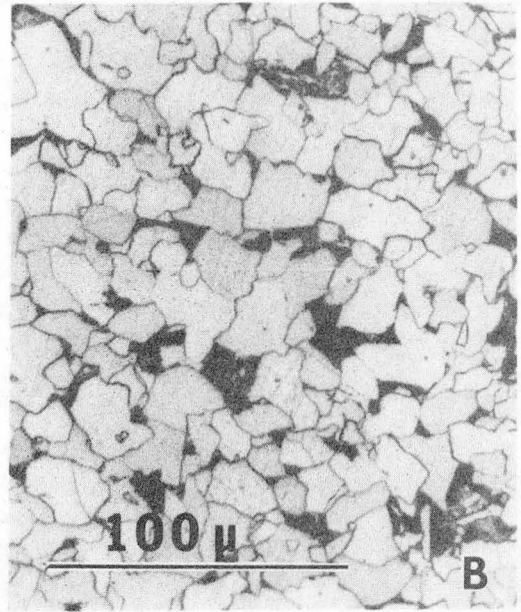
BASE                    BASE + V

AS RECEIVED

XBB 800-12387

Fig. 3

BASE                  BASE+V

800°C ICED BRINE QUENCH

XBB 800-12384

Fig. 4

1μ
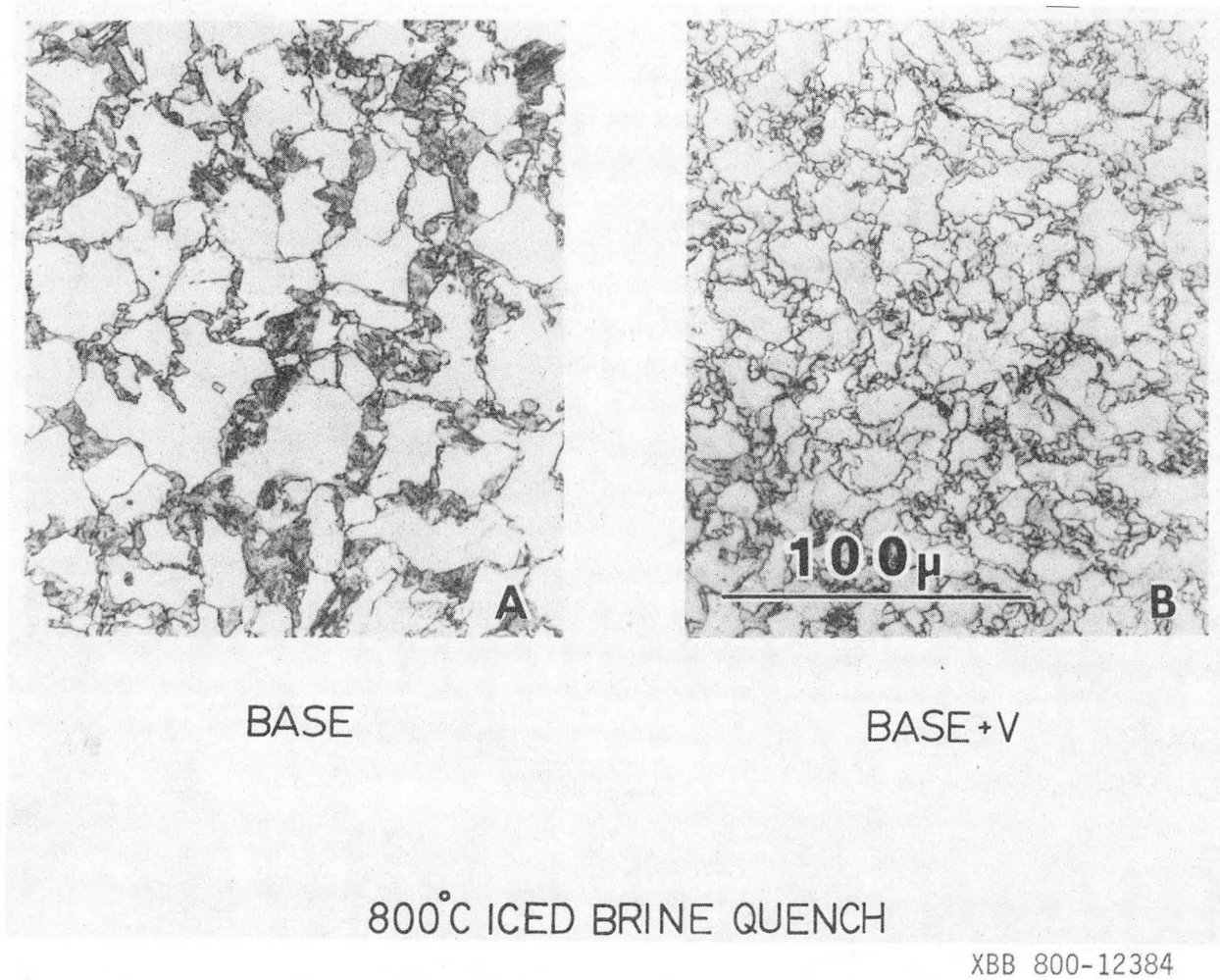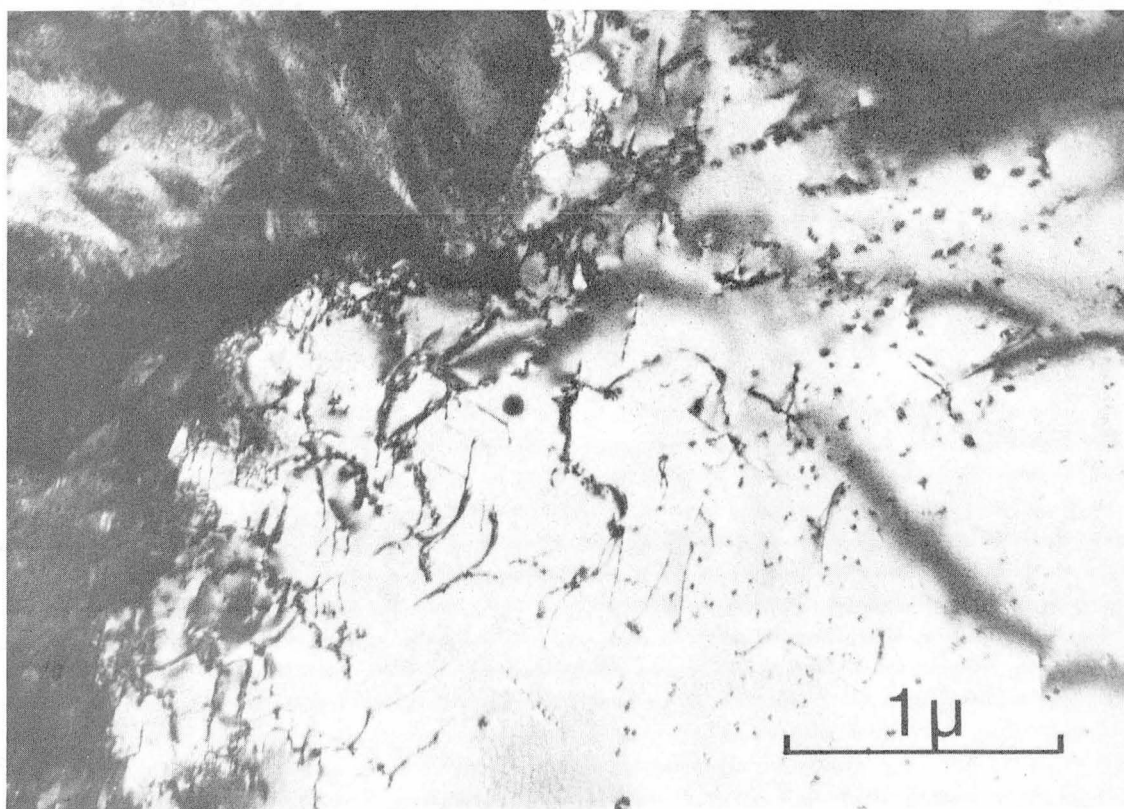
XBB 800-12390

Fig. 5

XBB 800-12389

Fig. 6

BASE                    BASE+V

800°C OIL QUENCH
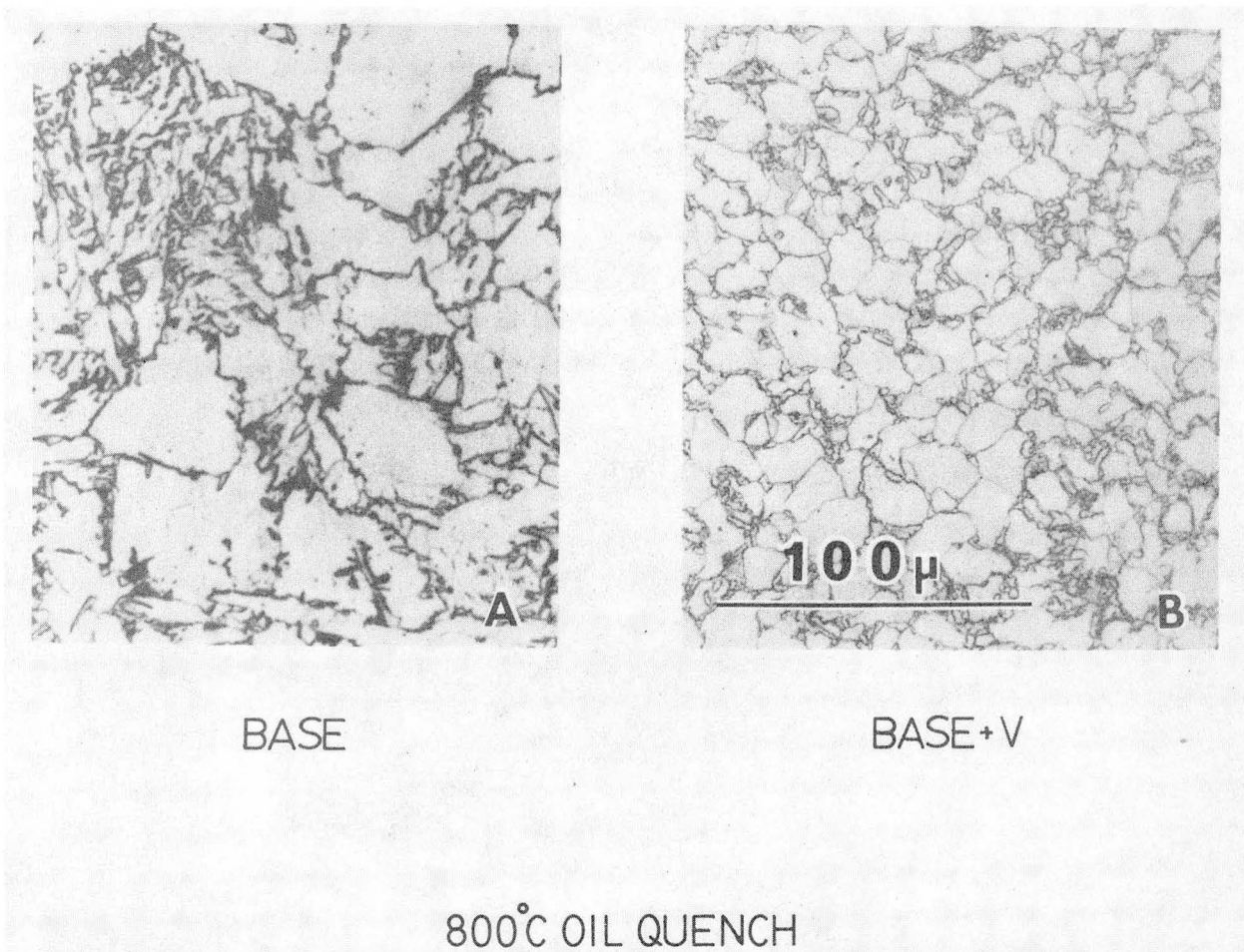
XBB 800-12385
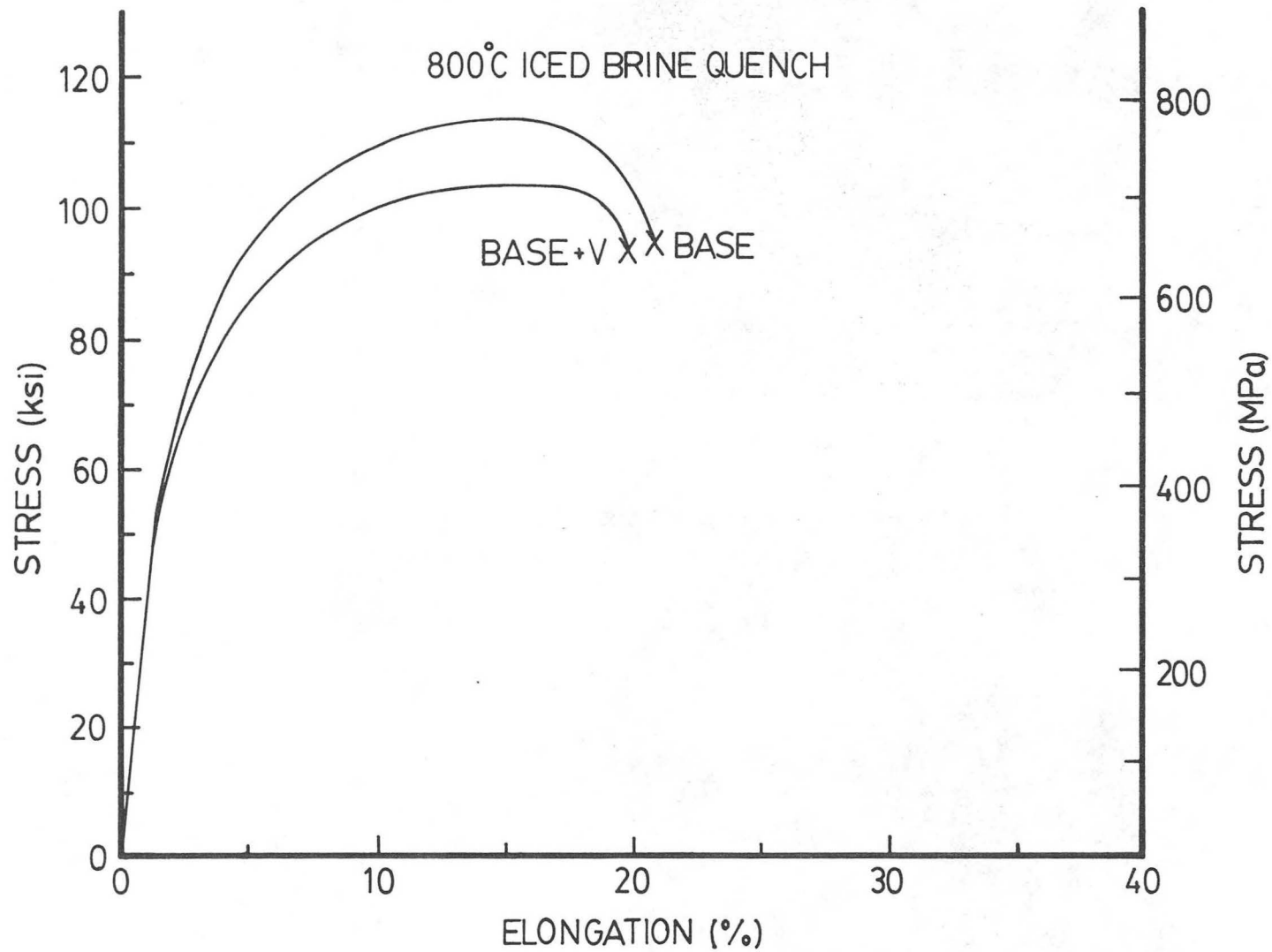
Fig. 7
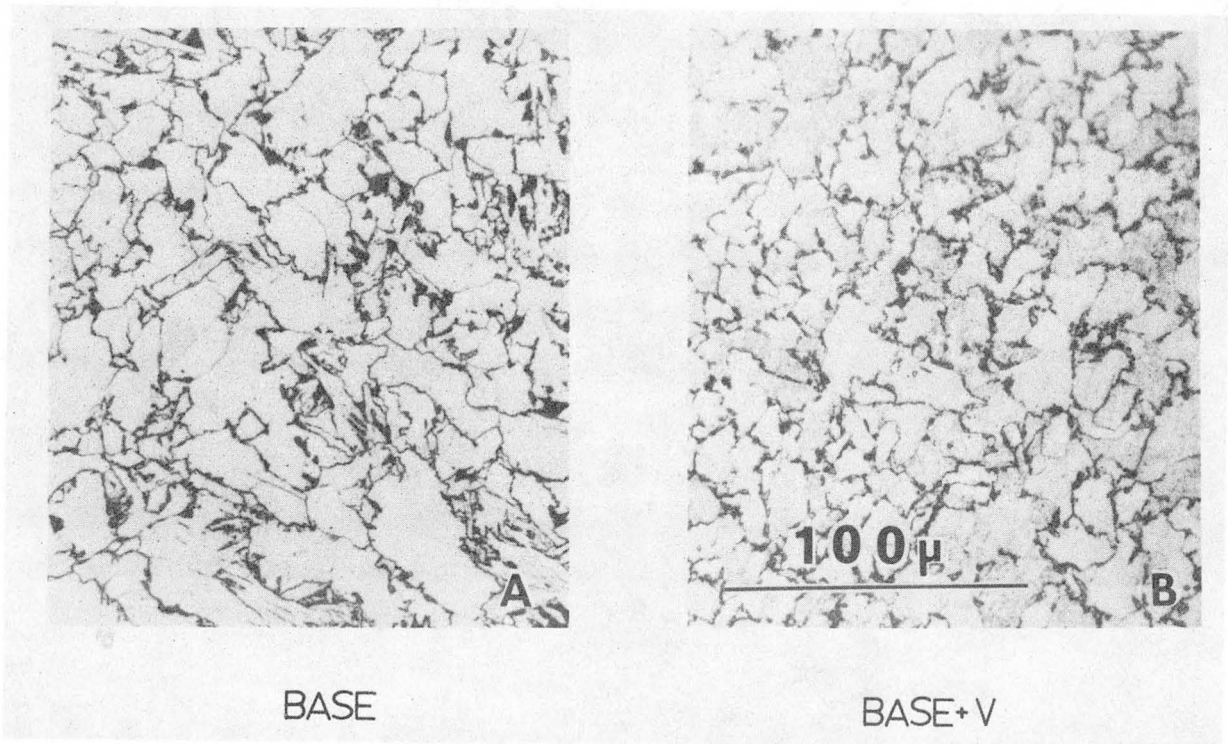
BASE                    BASE+V

800°C AIR COOL

Fig. 8
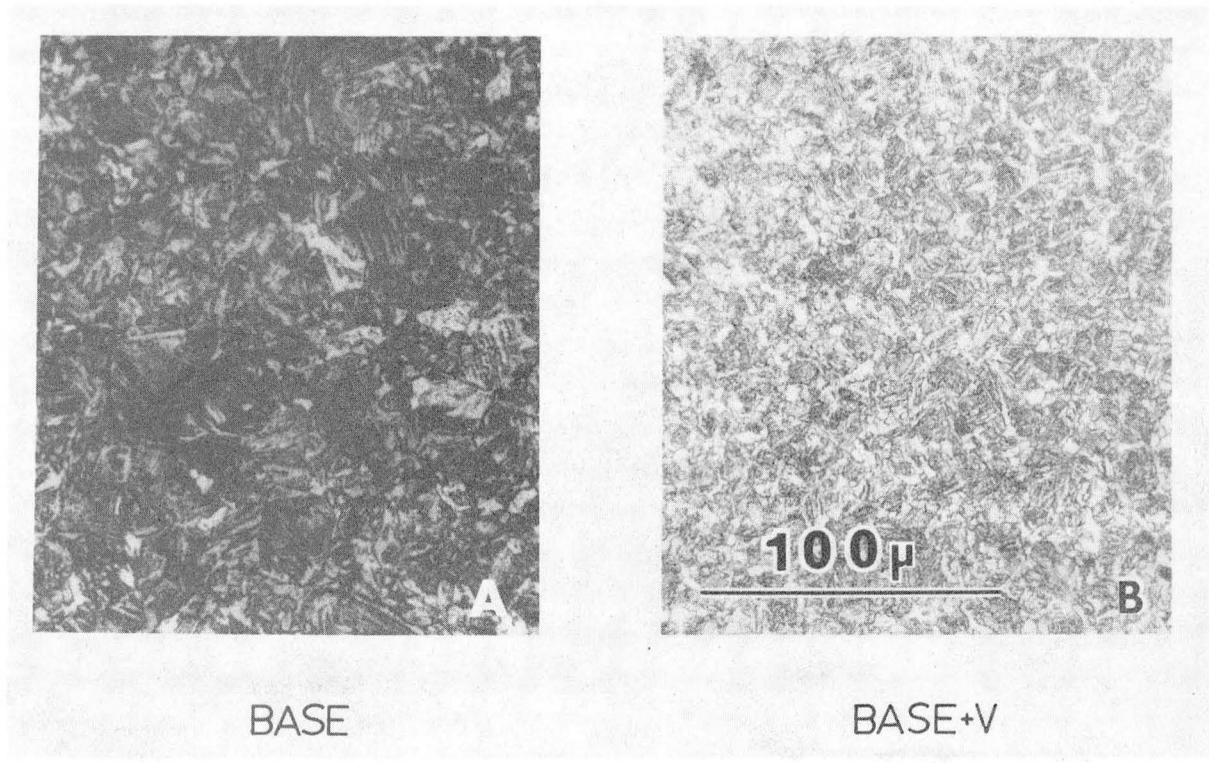
BASE            BASE+V

900°C OIL QUENCH

XBB 800-12388

Fig. 9

[101] Ferrite
[100] Cementite

XBB 800-14173
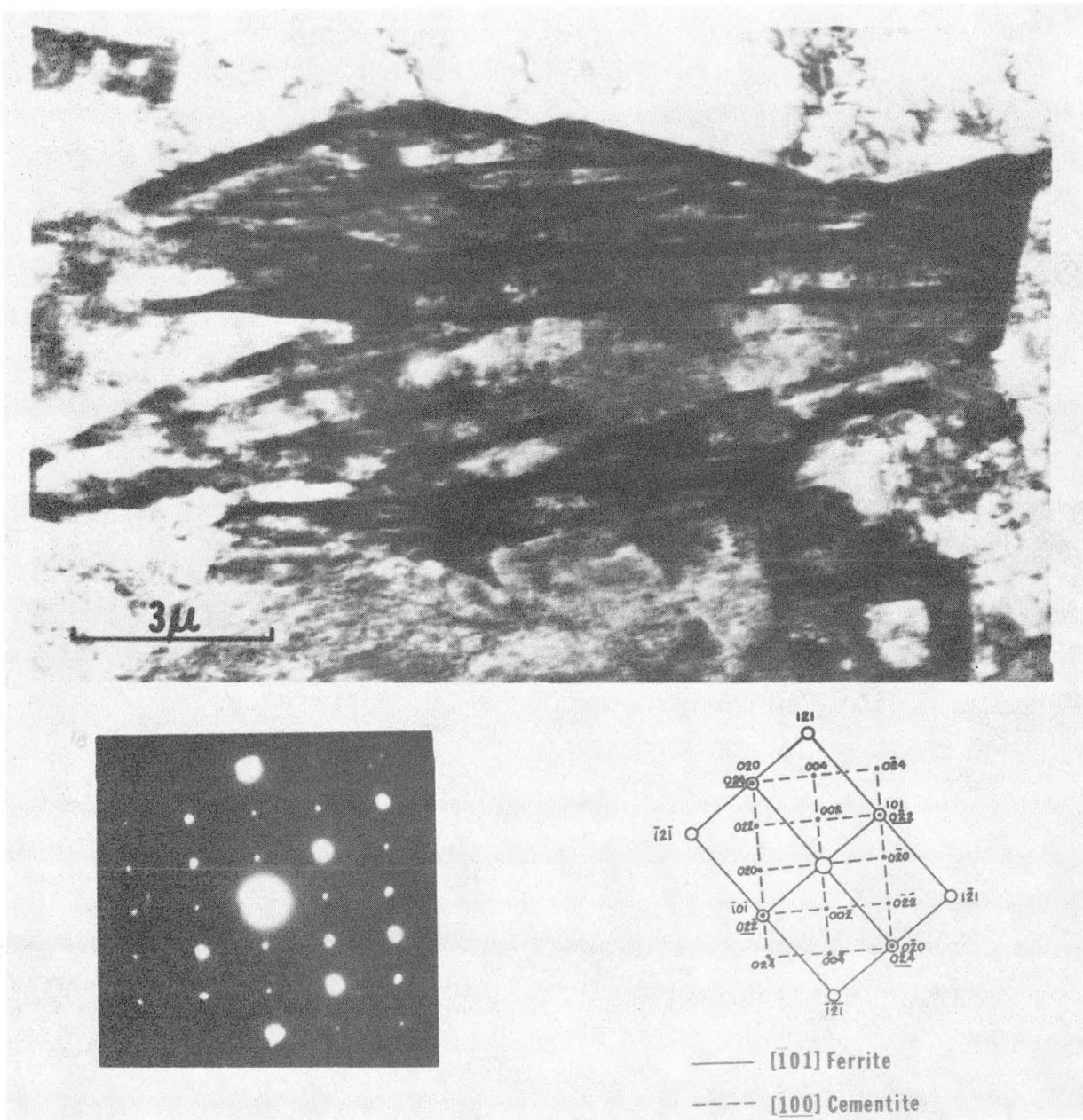
Fig. 10
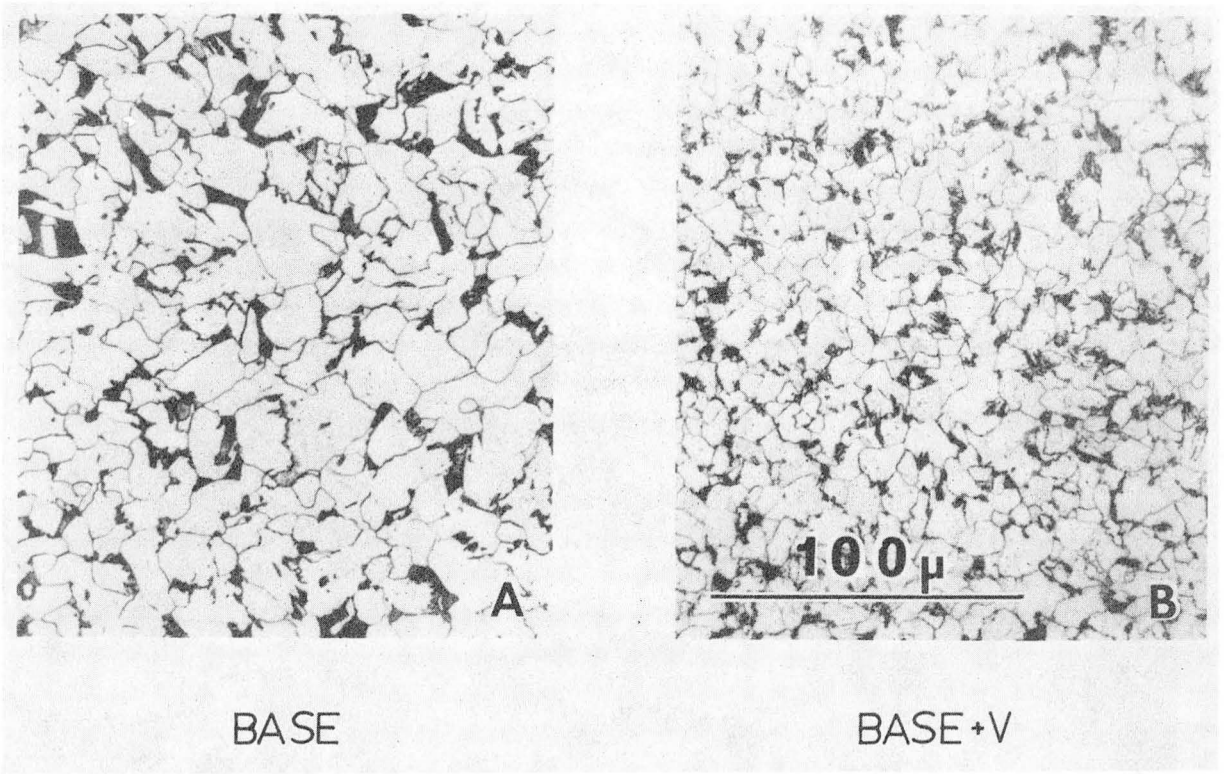
BASE           BASE+V

900°C AIR COOL

XBB 800-12383

Fig. 11
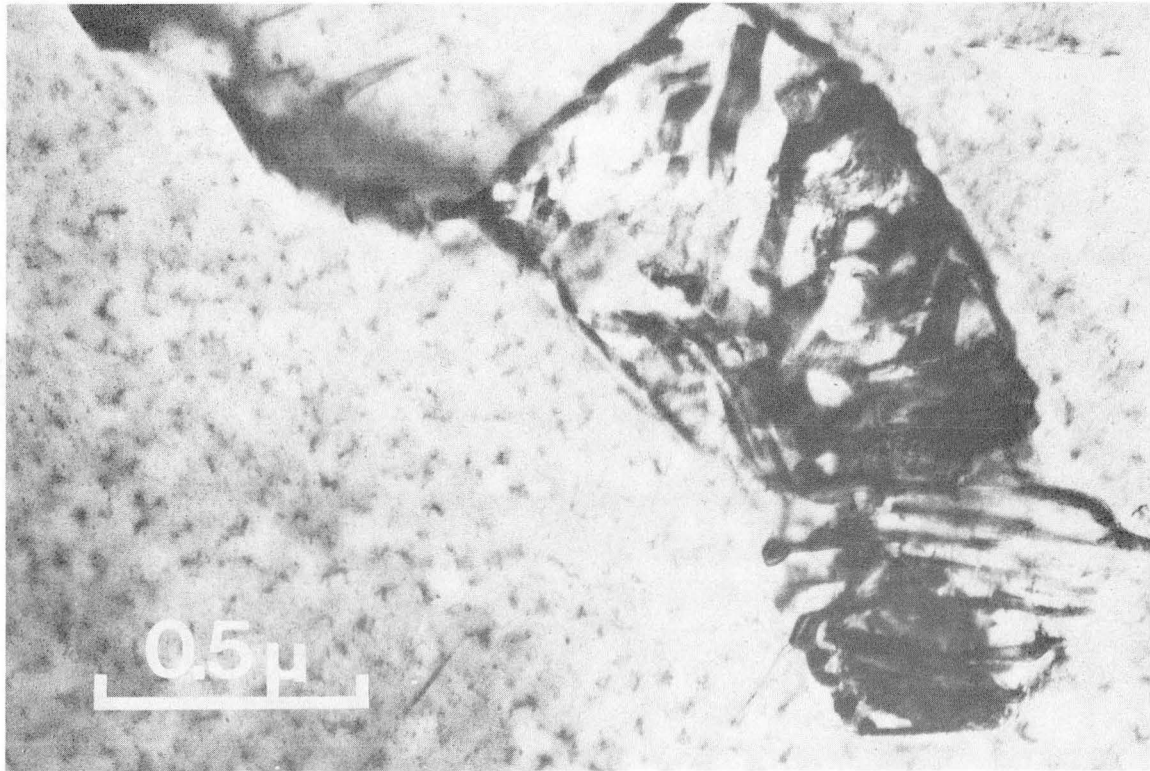
XBB 800-12394

Fig. 12
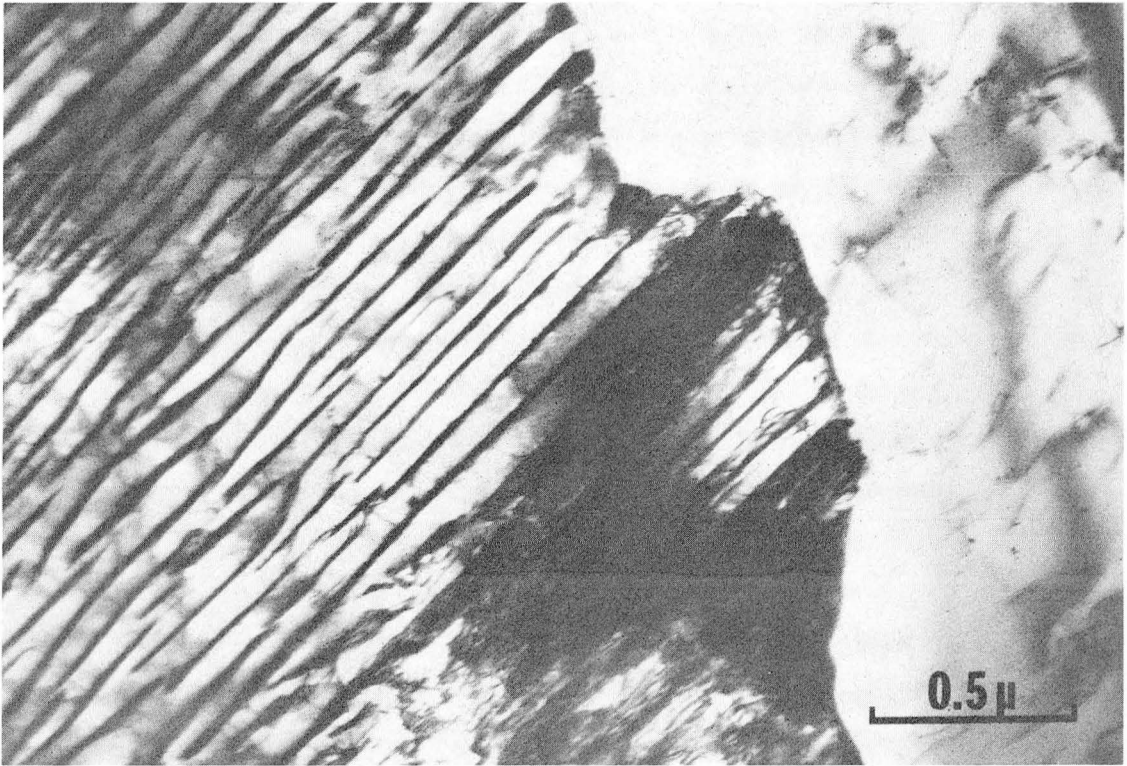
XBB 800-12391

Fig. 13
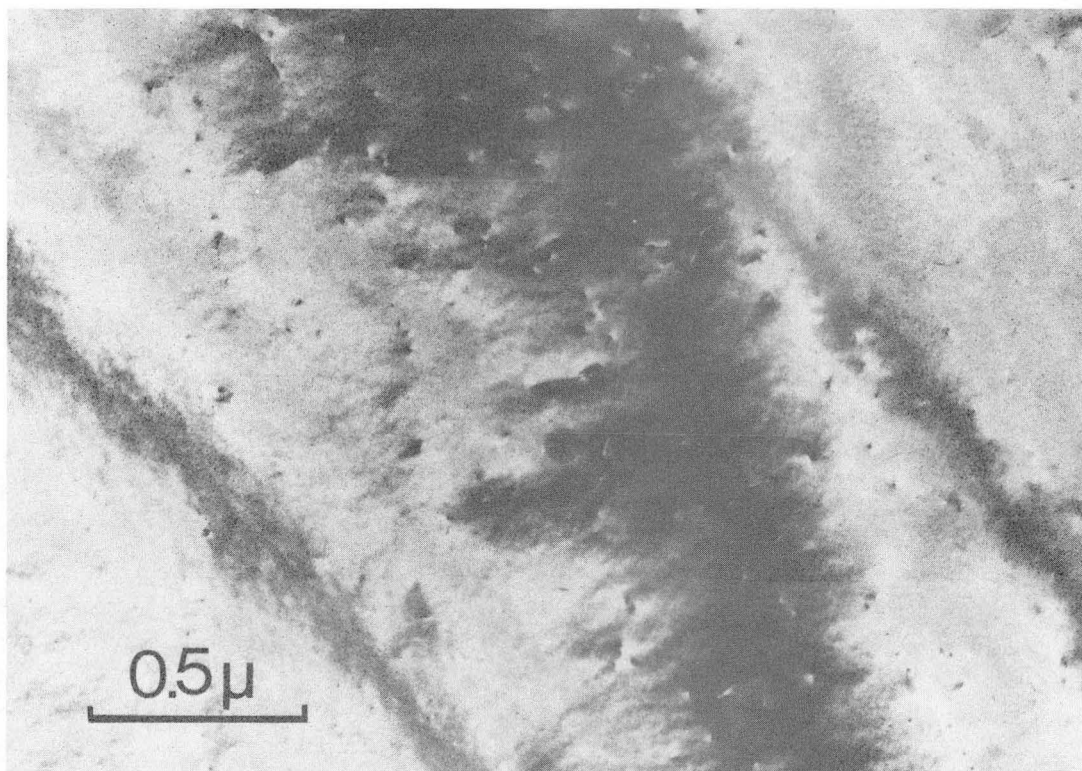
XBB 800-12392

Fig. 14
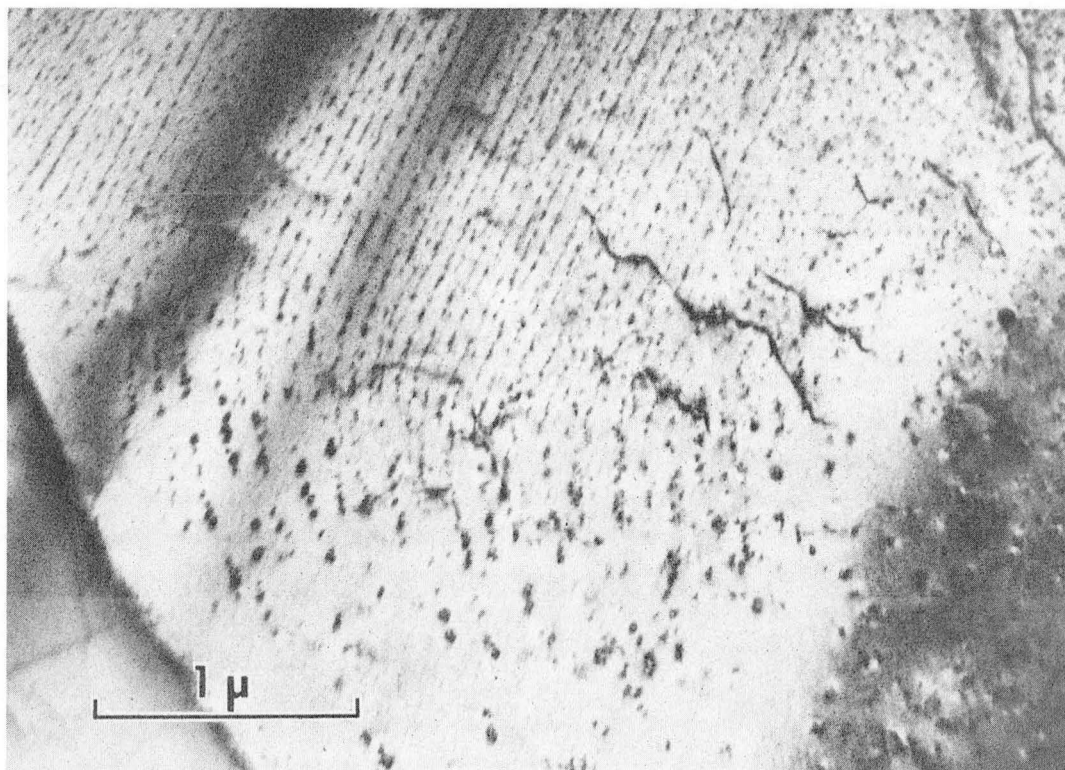
XBB 800-12393

Fig. 15

XBB 800-12395

Fig. 16
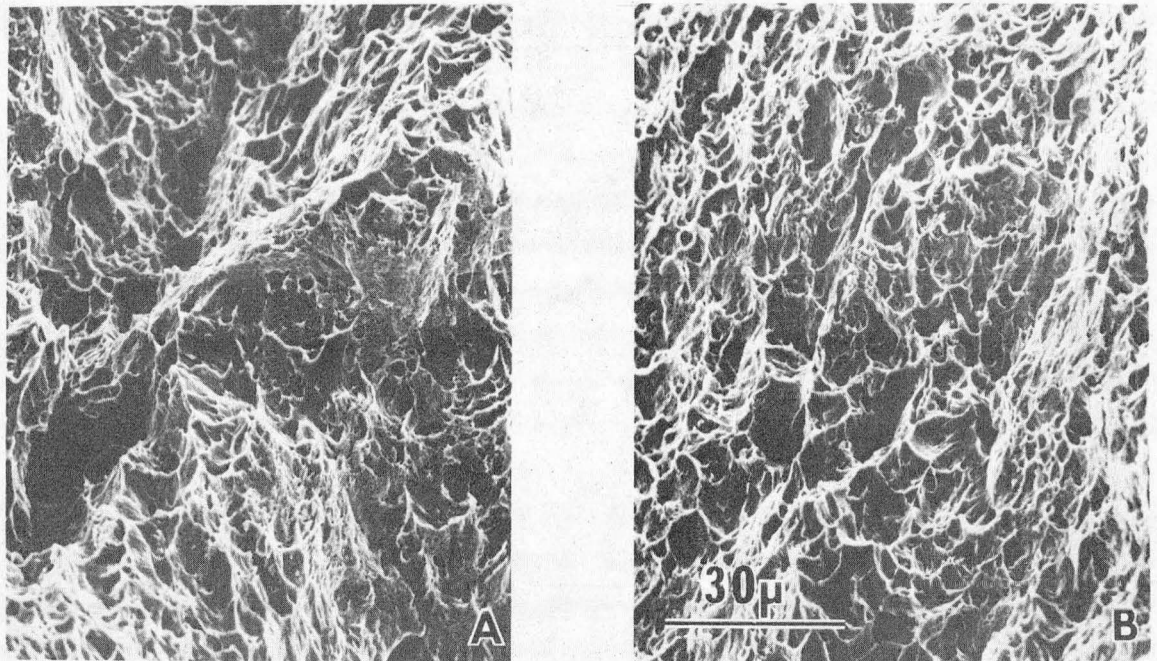
BASE            BASE+V

800°C ICED BRINE QUENCH

XBB 800-12382

Fig. 17

Fig. 18a

Fig. 18b

XBL 8011-7411

Fig. 18c

XBL 8011-7412

Fig. 18d

XBL 8011-7407

Fig. 18e

XBL 8011-7410